JACS
JOURNAL OF THE AMERICAN CHEMICAL SOCIETY

Communication

pubs.acs.org/JACS

Optically Modulated Photoswitchable Fluorescent Proteins Yield Improved Biological Imaging Sensitivity

Yen-Cheng Chen, Amy E. Jablonski, Irina Issaeva, Daisy Bourassa, Jung-Cheng Hsiang, Christoph J. Fahrni, and Robert M. Dickson*

School of Chemistry and Biochemistry and Petit Institute for Bioscience and Bioengineering, Georgia Institute of Technology, Atlanta, Georgia 30332-0400, United States

Supporting Information

ABSTRACT: Photoswitchable fluorescent proteins (PS-FPs) open grand new opportunities in biological imaging. Through optical manipulation of FP emission, we demonstrate that dual-laser modulated synchronously amplified fluorescence image recovery (DM-SAFIRe) improves signal contrast in high background through unambiguous demodulation and is linear in relative fluorophore abundance at different points in the cell. The unique bright-to-dark state interconversion rates of each PS-FP not only enables discrimination of different, yet spectrally indistinguishable FPs, but also allows signal rejection of diffusing relative to bound forms of the same PS-FP, rsFastLime. Adding to the sensitivity gains realized from rejecting non-modulatable background, the selective signal recovery of immobilized vs diffusing intracellular rsFastLime suggests that DM-SAFIRe can detect weak protein−protein interactions that are normally obscured by large fractions of unbound FPs.

Fluorescent proteins (FPs) are widely used to visualize and report on biological processes in live cells, tissues, and whole organisms.[1−4] While FPs offer good brightness, their detectability is too often limited by low copy numbers and high autofluorescent background.[4−6] Consequently, as fundamental limits exist on molecular brightness, imaging sensitivity is most readily improved through background reduction.[4−12] Practically, this can be achieved by using red-fluorescent proteins[6] to minimize autofluorescence or, more recently, by optically controlling emission intensity using either photoswitchable[7,12,13] or modulatable fluorophores.[11,13,14]

Although useful, photoswitch-based techniques to date have required incorporation of pure dye signals[7] to generate reference waveforms, or are slow due to being limited by the long natural lifetime of the "off" state.[12] Frequency domain imaging uses digital signal processing to better extract modulated signals, but is still limited by background from secondary excitation needed to recover the emissive photoswitch form.[13] To circumvent these limitations, we developed molecular modulation schemes that encode external modulation waveforms only on the desired fluorophore signals, thereby eliminating the need for internal reference dyes and enabling faster demodulated signal recovery. These synchronously amplified fluorescence image recovery (SAFIRe)[11,14] methods take advantage of select organic,[15] inorganic,[14,16] and FP labels[9,10] whose fluorescence intensity can be modulated through a dual-laser excitation scheme. While the primary laser excites all fluorescent molecules indiscriminately, a longer wavelength secondary laser regenerates fluorescence signals only of the SAFIRe-enabled fluorophores by selectively depopulating their transient dark states. Modulating this secondary laser thereby modulates only fluorescence of interest at a specific frequency. Demodulation-based SAFIRe thus enhances sensitivity by drastically reducing different yet spectrally indistinguishable background to yield >10-fold contrast improvements.[9,10]

Fluorophores used in SAFIRe exhibit transient dark states whose populations can be modulated by long-wavelength secondary excitation with any frequency that is slower than the characteristic dark-state decay. Because the molecular populations can be recovered prior to completion of a modulation cycle, the externally applied modulation frequency is directly encoded on the collected fluorescence to generate a linear overall signal recovery scheme that drastically improves contrast without generating any additional background. Importantly, even very low-yield dark states can be utilized in this scheme, as optically induced ground-state recovery yields fluorescent amplification. Most directly comparable with optical lock-in detection (OLID),[7,8] OLID relies on photoswitchable fluorescent proteins (PS-FPs), which are repeatedly cycled between cis (bright) and trans (dark) chromophore states through reversible bleaching upon alternating exposure to two high-energy lasers. Initially demonstrated with the well-characterized PS-FP Dronpa,[17] repetitive photoconversion between the ground and long-lived dark states can be effected with fluorescence excitation near 503 nm and dark-state excitation at ∼400 nm (Figure 1A). In OLID, even though both excitation sources generate background in the lower-energy fluorescence detection window, correlation of pure PS-FP photoswitching traces with each pixel-based intensity trajectory improves fluorescence imaging by enhancing bulk contrast over background.[7] The correlation with reference signals, however, is nonlinear with respect to fluorophore concentration,[7,8] and could lead to difficulties in image quantification.

The reversibly photoswitchable FP rsFastLime (Dronpa/V157G)[18] combines a large fluorescence quantum yield (Φ = 0.6)[19] with efficient forward and reverse photoisomerization of

Received: July 27, 2015
Published: September 24, 2015

DOI: 10.1021/jacs.5b07871
J. Am. Chem. Soc. 2015, 137, 12764−12767

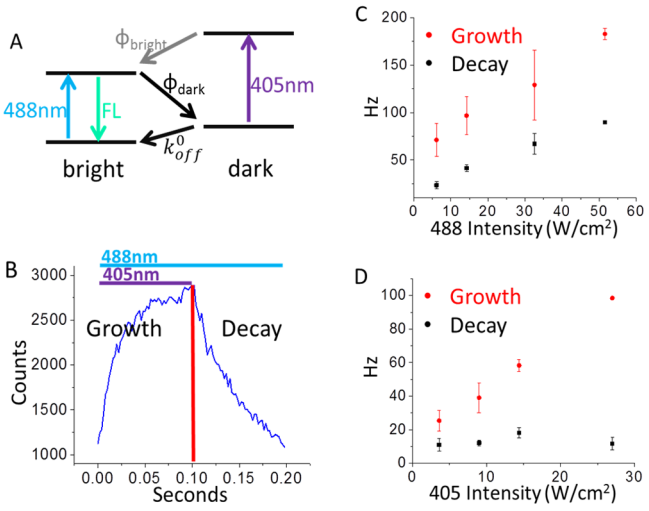

$$\textbf{Growth: } k_{on} + k_{off} = I_{488}\sigma_{488}\Phi_{dark}\frac{1}{h\nu} + k^0_{off} + I_{405}\sigma_{405}\Phi_{bright}\frac{1}{h\nu}$$

$$\textbf{Decay: } k_{on} + k^0_{off} = I_{488}\sigma_{488}\Phi_{dark}\frac{1}{h\nu} + k^0_{off}$$

Figure 1. Photophysics of the photoswitchable protein rsFastLime (Dronpa-V157G). (A) Schematic of transitions between the bright- and the dark-state manifolds, with ~518 nm fluorescence resulting from 488 nm excitation. Excitation at 405 nm depopulates the dark state and regenerates the bright manifold. (B) Continuous 488 nm and modulated 405 nm excitations yield fluorescence time traces showing exponential growth and decay. The growth is a function of the 488 nm-induced rate into the dark state (k_{on}), the thermal relaxation rate (k_{off}^0), and the 405 nm-induced dark-state depopulation rate ($I_{405}\sigma^{405}{}_{bright}\Phi_{Rev}$), while the decay is a similar function without the 405 nm-induced rate. (C) Plotting the growth and decay rates vs the intensity at 488 nm yields the corresponding rate constants into (slope) and out of (intercept) the dark state. The 405 nm intensity is 14.4 W/cm^2. (D) The intercepts of (C) from various 405 nm laser intensities are linear in both growth and decay plots.

a high-energy-absorbing dark state.[17−19] For wide-field imaging with a charge-coupled device, the high contrast at low modulation frequencies makes rsFastLime nearly ideal for photoswitch-based imaging. We measured the bright- and dark-state lifetimes by analyzing the transient response of rsFastLime to continuous-wave 488 nm (primary) excitation and modulated 405 nm (secondary) co-illumination (Figure 1B). Exponential fits to the fluorescence decays yielded the rates into (k_{on}) and out of (k_{off}) the dark state.[11] Coupled with the known absorption cross section (σ_{488}),[18,19] the slopes of the decay and growth rates vs primary excitation intensity (Figure 1C) gave a dark-state quantum yield of Φ_{dark} = 0.0035, while the intercept of growth rate vs secondary excitation intensity (Figure 1D) gave $\sigma_{405}\Phi_{Rev}$ = 1.6 × 10^{-18} cm^2. Thus, while rsFastLime still offers bright emission, its dark-state quantum yield is ~10 times larger than that of Dronpa,[18,19] which should lead to improved contrast upon photoswitching. Although PS-FPs dark states are much longer-lived and are depopulated only with high-energy excitation, the forward and reverse photoisomerization rates can be controlled by the primary and secondary laser intensities. Thus, PS-FPs can be used in SAFIRe-like modulation schemes, with the caveat that, like OLID, both signal and background will be modulated.

To generate a direct comparison for fluorescence image recovery, we employed both OLID and SAFIRe with dual high-energy lasers using rsFastLime. Although autofluorescent background is induced upon secondary laser illumination, OLID uses short bursts of high energy secondary excitation to regenerate the emissive state, while SAFIRe allows for either secondary-only or both primary and secondary modulation (i.e., single-laser modulation, SM, and dual-laser modulation, DM, respectively), typically using 50% duty cycles. While background is independently modulated at both primary and secondary modulation frequencies, only the rsFastLime emission is affected by the product of both lasers (see Supporting Information). Thus, secondary-only modulation and DM-SAFIRe offer direct recovery of rsFastLime fluorescence. With DM, only rsFastLime signals are modulated at the sum and difference of the primary and secondary modulation frequencies, completely excluding autofluorescent background from these sideband signals (Figure 2). Even

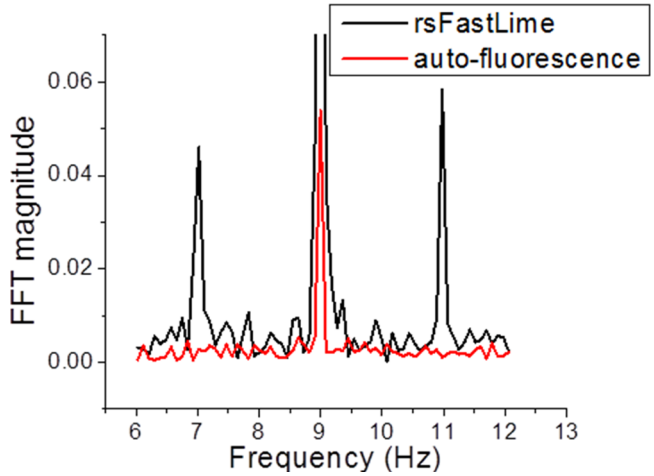

Figure 2. Dual modulation enables background-free rsFastLime detection. rsFastLime interacts with both 405 and 488 nm lasers, while autofluorescence background is excited independently by each laser. The Fourier transform shows that only rsFastLime presents sideband signals (7 and 11 Hz) when 488 nm is modulated at 9 Hz and 405 nm at 2 Hz.

though 405 nm can weakly excite emission from the bright state as well, the sideband signals at the sum and difference of 488 and 405 nm modulation frequencies appear without signals from 405 nm-only excitation.

For imaging live cells, we co-transfected adherent NIH 3T3 mouse fibroblast cells with untargeted EGFP and rsFastLime fused to a mitochondrial targeting sequence. Upon modulating 488 and 405 nm lasers at different frequencies, we reconstructed the SAFIRe images from an image sequence by plotting the amplitude at each sum or difference of the two modulation frequencies. Secondary-only SM-SAFIRe images were also recovered from the amplitude at the 405 nm laser modulation frequency. Both SM and DM reveal the mitochondria devoid of EGFP background, but SM shows higher autofluorescent background compared to DM (Figure 3A).

Compared to SAFIRe, OLID utilizes a slightly different excitation scheme involving cross-correlation of each pixel with a bright, "pure" dye reference signal that must be identified within each sample. To facilitate image recovery, OLID analysis was recently automated by using the brightest feature within an image sequence as the internal reference.[8] Because OLID

DOI: 10.1021/jacs.5b07871
J. Am. Chem. Soc. 2015, 137, 12764−12767

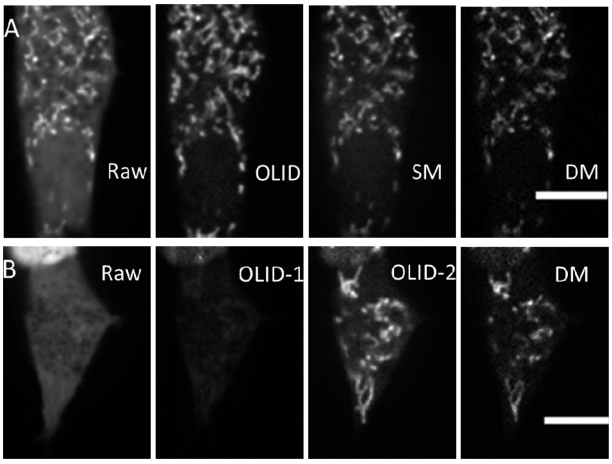

Figure 3. (A) Signal/background (S/B) comparison of SM- and DM-SAFIRe vs OLID in live NIH-3T3 cells co-expressing untargeted EGFP and mitochondria-targeted rsFastLime: (left to right) raw image, S/B ≈ 1.4; OLID, S/B ≈ 6; demodulated image at 405 nm frequency (SM-SAFIRe), S/B ≈ 5; demodulation at the sideband frequencies (DM-SAFIRe), S/B ≈ 9. (B) S/B comparison in the presence of bright non-rsFastLime background: (left to right) raw live cell image as in (A), S/B ≈ 1; OLID using automatic selection of brightest feature for reference waveform, S/B ≈ 1.6; OLID with manual selection of reference point, S/B ≈ 5; demodulation image upon DM-SAFIRe, S/B ≈ 9. Scale bars = 10 μm. OLID and SM-SAFIRe give similar contrast improvements, and DM-SAFIRe gives a further 2-fold improvement.

reconstruction multiplies each individual pixel intensity trajectory by that of the reference pixel trajectory, and each is normalized by its respective standard deviation of intensity values,[7,8] OLID scales nonlinearly with the number of fluorophores at each position in the image, thus distorting the true contrast among emissive species. Further, in high background environments or if the position of the reference signal is not well-defined, OLID automation can select the wrong reference point, thereby drastically reducing contrast (Figure 3B, OLID-1 vs OLID-2). Unlike OLID, SM- and DM-SAFIRe are linear and represent true relative fluorophore amounts.

Although the 405 nm duty cycle is higher with SAFIRe, leading to higher background in the raw images, both SM-SAFIRe and OLID[7,8] can produce images with similar apparent contrast improvements (Figure 3A). The external modulation of SAFIRe with Fourier reconstruction, however, ensures both linearity in image recovery and no ambiguity in the reference signal.[11] In fact, as OLID utilizes short, repeated bursts of 405 nm laser exposure, one can simply analyze OLID data by plotting each pixel amplitude at the burst frequency to generate a linear, SAFIRe-like image (Figure S1). DM-SAFIRe, which recovers signal from the sum and difference of primary and secondary modulation frequencies, further eliminates contributions arising from the 405 nm-induced autofluorescence. This results in an additional 2-fold increase in linear signal discrimination over both SM-SAFIRe and OLID. Thus, the contrast improvements and linearity in signal recovery (from the Fourier transform) provides distinct advantages of SAFIRe over other signal recovery schemes, even when using PS-FPs with two high-energy lasers for excitation.

The ability to tune SAFIRe modulation frequency relative to the excitation intensity-dependent dark-state population and depopulation rates in PS-FPs (e.g., rsFastLime) affords new modes for protein discrimination, unavailable to other signal recovery schemes. Under the low 488 nm (<10 W/cm^2) and 405 nm (~4 W/cm^2) intensities used here, the time scale to establish the steady-state rsFastLime dark-state population is significantly longer than the diffusional transit time through a focused laser spot. Thus, diffusing molecules do not reside sufficiently long within the focal volume to generate either SM-SAFIRe or DM-SAFIRe signals. While SM-SAFIRe generates autofluorescent background from high-energy secondary excitation, DM-SAFIRe shows neither autofluorescent background nor signals of diffusing rsFastLime molecules (Figure 4). In live cells, the estimated diffusion time for proteins is ~10

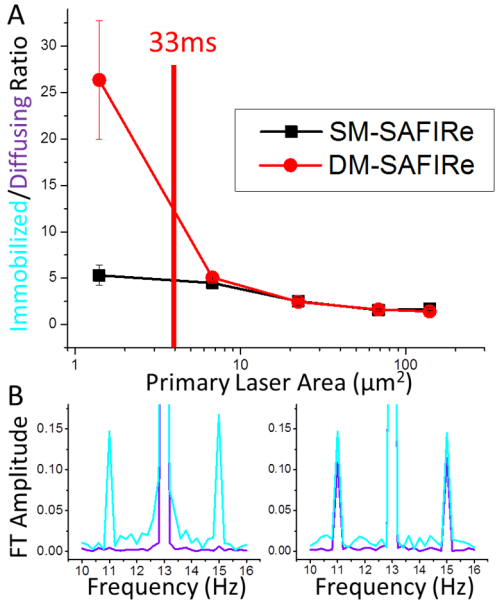

Figure 4. Contrast between localized mito-rsFastLime vs freely diffusing rsFastLime with varying excitation area. (A) Increasing the laser spot size (intensity constant at 7 W/cm^2, 488 nm, and at 3 W/cm^2, 405 nm) increases the diffusion time of untargeted-rsFastLime, allowing diffusing rsFastLime to be modulated. Thus, the ratio of immobilized to diffusing molecules approaches unity in dual modulation (DM), while the ratio using single modulation (SM) suffers from higher autofluorescent background. The ratio in SM (~5) is much smaller than that achieved with DM (~25) with small excitation area. The major change is seen when the diffusional transit time of untargeted rsFastLime increases beyond the 33 ms photophysical time scale. (B) Left, immobilized (blue) and diffusing (purple) rsFastLime DM-SAFIRe signals using a ~1.4 μm^2 excitation area; right, the same DM-SAFIRe signals using a ~140 μm^2 excitation area.

ms (laser spot radius: 0.67 μm), which is significantly shorter than the ~33 ms dark-state lifetime (at 7 W/cm^2, 488 nm, and at 3 W/cm^2, 405 nm, Figure 4). Hence, the diffusion-rate-dependent signal amplitude should allow for distinguishing bound vs diffusing rsFastLime while simultaneously eliminating un-modulatable background.

Comparing sideband intensities in DM-SAFIRe within cells expressing either untargeted, freely diffusing rsFastLime, or targeted mito-rsFastLime, it can be seen that sideband amplitudes (i.e., modulation depth) decrease with decreasing excitation volume. The sideband amplitude ratio of signals from localized mito-rsFastLime vs those from freely diffusing rsFastLime reaches 1 only in large excitation volumes, in which diffusion rates are not fast relative to photophysical rates.

DOI: 10.1021/jacs.5b07871
J. Am. Chem. Soc. 2015, 137, 12764−12767

This demonstrates that we can use the different modulation frequency responses of bound and unbound molecules for selective visualization of targeted rsFastLime, with potentially >25-fold selectivity over diffusing, but otherwise identical rsFastLime.

Taking advantage of the above relationship between modulation frequency and spot size, we preferentially recovered signals from mitochondria-localized rsFastLime relative to untargeted rsFastLime in live cells co-expressing the two forms of the same FP (Figure 5). Even with few-μm spot

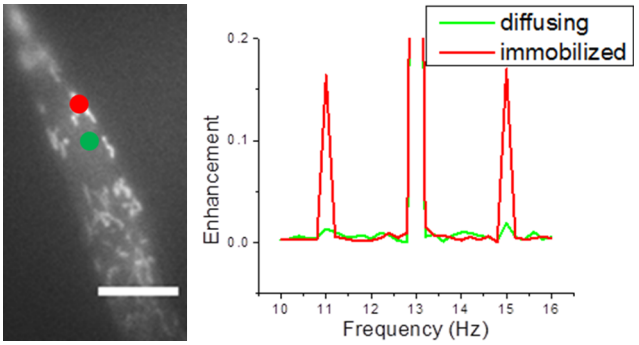

Figure 5. Diffusing vs immobilized rsFastLime in cells co-expressing mito-rsFastLime and untargeted-rsFastLime. The ratio of the immobilized to diffusing molecules is ~10. 488 nm is 8.8 W/cm^2 modulated at 13 Hz, and 405 nm is 2.4 W/cm^2 modulated at 2 Hz. Scale bar = 10 μm.

diameters, DM readily increased the signal of molecules residing longer within the laser focal volume. While fluorescence correlation spectroscopy (FCS), fluorescence recovery after photobleaching (FRAP), and Förster resonance energy transfer (FRET) have difficulty in visualizing weak protein−protein interactions in vivo,[20−22] rsFastLime modulation depth should enhance contrast of bound molecules over transiently diffusing molecules, especially in very small focal volumes.

Over the past decade, photoswitchable fluorescent proteins have played a key role in developing new imaging schemes for high-contrast imaging in live cells. Here, we have demonstrated the implementation of SAFIRe and dual modulation for *linear* contrast improvement in fluorescence imaging.[11] This externally applied modulation waveform is directly encoded on collected fluorescence, improving linearity and contrast over existing methods, while enabling extensions to discriminate signals from multiple fluorophores and enhancing contrast of immobilized species relative to the same proteins diffusing in cells. These potential applications of high-energy PS-FPs offer great potential for discriminating fluorophores of interest from otherwise identical PS-FPs that are merely in different environments to remove overwhelming background in live cell imaging, while simultaneously offering new opportunities for studying weak protein−protein interactions within live cells.

■ ASSOCIATED CONTENT

Supporting Information

The Supporting Information is available free of charge on the ACS Publications website at DOI: 10.1021/jacs.5b07871.

Experimental methods, data analysis, derivation of photophysical response for SM- and DM-SAFIRe, and recovered images using SM-/DM-SAFIRe and OLID schemes (PDF)

■ AUTHOR INFORMATION

Corresponding Author

*dickson@chemistry.gatech.edu

Notes

The authors declare no competing financial interest.

■ ACKNOWLEDGMENTS

The authors gratefully acknowledge support from NIH R21EB020371 and NIH R21EB009976.

■ REFERENCES

(1) Tsien, R. Y. *Annu. Rev. Biochem.* **1998**, *67*, 509−544.
(2) Zimmer, M. *Chem. Rev.* **2002**, *102*, 759−782.
(3) Lippincott-Schwartz, J.; Patterson, G. H. *Science* **2003**, *300*, 87−91.
(4) Giepmans, B. N. G.; Adams, S. R.; Ellisman, M. H.; Tsien, R. Y. *Science* **2006**, *312*, 217−224.
(5) Billinton, N.; Knight, A. W. *Anal. Biochem.* **2001**, *291*, 175−197.
(6) Shcherbakova, D. M.; Subach, O. M.; Verkhusha, V. V. *Angew. Chem., Int. Ed.* **2012**, *51*, 10724−10738.
(7) Marriott, G.; Mao, S.; Sakata, T.; Ran, J.; Jackson, D. K.; Petchprayoon, C.; Gomez, T. J.; Warp, E.; Tulyathan, O.; Aaron, H. L.; Isacoff, E. Y.; Yan, Y. *Proc. Natl. Acad. Sci. U. S. A.* **2008**, *105*, 17789−17794.
(8) Du, G.; Marriott, G.; Yan, Y. *Bioinfor. Biomed. Eng. (iCBBE), 2010 4th International Conference* **2010**, 1−5.
(9) Jablonski, A. E.; Hsiang, J. C.; Bagchi, P.; Hull, N.; Richards, C. I.; Fahrni, C. J.; Dickson, R. M. *J. Phys. Chem. Lett.* **2012**, *3*, 3585−3591.
(10) Jablonski, A. E.; Vegh, R. B.; Hsiang, J. C.; Bommarius, B.; Chen, Y. C.; Solntsev, K. M.; Bommarius, A. S.; Tolbert, L. M.; Dickson, R. M. *J. Am. Chem. Soc.* **2013**, *135*, 16410−16417.
(11) Hsiang, J. C.; Jablonski, A. E.; Dickson, R. M. *Acc. Chem. Res.* **2014**, *47*, 1545−1554.
(12) Querard, J.; Markus, T. Z.; Plamont, M. A.; Gauron, C.; Wang, P.; Espagne, A.; Volovitch, M.; Vriz, S.; Croquette, V.; Gautier, A.; Le Saux, T.; Jullien, L. *Angew. Chem., Int. Ed.* **2015**, *54*, 2633−2637.
(13) Li, A. D.; Zhan, C.; Hu, D.; Wan, W.; Yao, J. *J. Am. Chem. Soc.* **2011**, *133*, 7628−7631.
(14) Richards, C. I.; Hsiang, J. C.; Senapati, D.; Patel, S.; Yu, J. H.; Vosch, T.; Dickson, R. M. *J. Am. Chem. Soc.* **2009**, *131*, 4619−4621.
(15) Fan, C.; Hsiang, J. C.; Dickson, R. M. *ChemPhysChem* **2012**, *13*, 1023−1029.
(16) Petty, J. T.; Fan, C.; Story, S. P.; Sengupta, B.; Sartin, M.; Hsiang, J. C.; Perry, J. W.; Dickson, R. M. *J. Phys. Chem. B* **2011**, *115*, 7996−8003.
(17) Ando, R.; Mizuno, H.; Miyawaki, A. *Science* **2004**, *306*, 1370−1373.
(18) Stiel, A. C.; Trowitzsch, S.; Weber, G.; Andresen, M.; Eggeling, C.; Hell, S. W.; Jakobs, S.; Wahl, M. C. *Biochem. J.* **2007**, *402*, 35−42.
(19) Andresen, M.; Stiel, A. C.; Folling, J.; Wenzel, D.; Schonle, A.; Egner, A.; Eggeling, C.; Hell, S. W.; Jakobs, S. *Nat. Biotechnol.* **2008**, *26*, 1035−1040.
(20) Sprague, B. L.; Pego, R. L.; Stavreva, D. A.; McNally, J. G. *Biophys. J.* **2004**, *86*, 3473−3495.
(21) Benitez, J. J.; Keller, A. M.; Ochieng, P.; Yatsunyk, L. A.; Huffman, D. L.; Rosenzweig, A. C.; Chen, P. *J. Am. Chem. Soc.* **2008**, *130*, 2446−2447.
(22) Benítez, J. J.; Keller, A. M.; Chen, P. *Methods Enzymol.* **2010**, *472*, 41−60.

DOI: 10.1021/jacs.5b07871
J. Am. Chem. Soc. 2015, 137, 12764−12767